A phonon laser operating at an exceptional point

Jing Zhang[1,2,3,10], Bo Peng[1,8,10], Şahin Kaya Özdemir[1,9], Kevin Pichler[4], Dmitry O. Krimer[4], Guangming Zhao[1], Franco Nori [5,6], Yu-xi Liu[3,7], Stefan Rotter [4] and Lan Yang [1]*

[1]Department of Electrical and Systems Engineering, Washington University, St Louis, MO, USA. [2]Department of Automation, Tsinghua University, Beijing, China. [3]Center for Quantum Information Science and Technology, BNRist, Beijing, China. [4]Institute for Theoretical Physics, Vienna University of Technology (TU Wien), Vienna, Austria. [5]Theoretical Quantum Physics Laboratory, RIKEN, Saitama, Japan. [6]Physics Department, The University of Michigan, Ann Arbor, MI, USA. [7]Institute of Microelectronics, Tsinghua University, Beijing, China. [8]Present address: IBM Thomas J. Watson Research Center, Yorktown Heights, NY, USA. [9]Present address: Department of Engineering Science and Mechanics, The Pennsylvania State University, University Park, PA, USA. [10]These authors contributed equally: Jing Zhang, Bo Peng. *e-mail: yang@seas.wustl.edu

Supplementary Information – A phonon laser operating at an exceptional point

Jing Zhang[1,2,3], Bo Peng[1 †], Şahin Kaya Özdemir[1 †], Kevin Pichler[4], Dmitry O. Krimer[4], Guangming Zhao[1], Franco Nori[5,6], Yu-xi Liu[3,7], Stefan Rotter[4], & Lan Yang[1*]

Affiliations:

[1]Department of Electrical and Systems Engineering, Washington University, St. Louis, Missouri 63130, USA

[2]Department of Automation, Tsinghua University, Beijing 100084, P. R. China

[3]Center for Quantum Information Science and Technology, BNRist, Beijing 100084, P. R. China

[4]Institute for Theoretical Physics, Vienna University of Technology (TU Wien), Vienna, Austria, EU

[5]Theoretical Quantum Physics Laboratory, RIKEN, Saitama 351-0198, Japan

[6]Physics Department, The University of Michigan, Ann Arbor, MI 48109-1040, USA

[7]Institute of Microelectronics, Tsinghua University, Beijing 100084, P. R. China

[†]Present address: IBM Thomas J. Watson Research Center, Yorktown Heights, New York 10598, USA (B.P.); Department of Engineering Science and Mechanics, The Pennsylvania State University, University Park, Pennsylvania 16802 USA (S.K.O.).

*email: yang@seas.wustl.edu

I.   EXPERIMENTAL SETUP

Our experiment was performed using the setup illustrated in Fig. S1. An optical probe field provided by a tunable External Cavity Laser Diode (ECLD) in the 1550 nm band was fed into the fiber. A section of the fiber was tapered to enable efficient coupling of the probe field into and out of a microtoroid resonator, which is coupled to another microtoroid resonator with tunable damping rate induced by a chromium (Cr)-coated silica-nanofiber tip with strong absorption rate of light in the 1550-nm band, and the output field was sent to a Photo-Detector (PD). The electrical signal from the PD was then analyzed
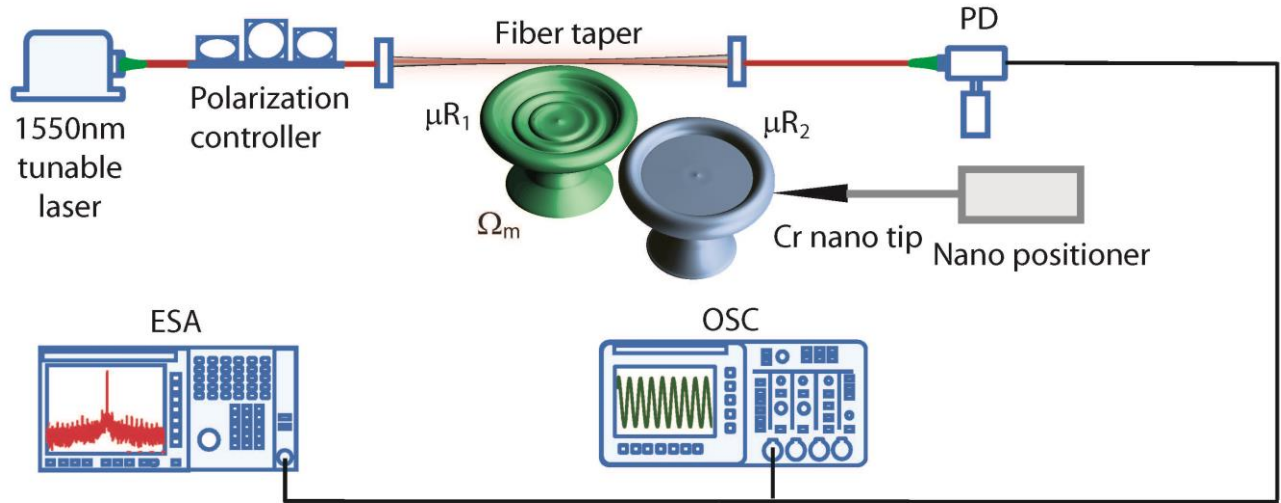

Figure S1. Schematic diagram of the experimental setup. The 1550 nm laser is fed into two coupled microtoroid resonators μR1 and μR2. The first resonator μR1 supports a high-Q optical mode a_1 and a mechanical mode with frequency Ω_m, while the second resonator μR2 supports a low-Q mode a_2. The damping rate of the low-Q mode a_2 is tuned by a Cr-coated silica nanotip touching the resonator μR2. The output signal is detected by a photodetector and then fed into the oscilloscope and the electrical spectrum analyzer to obtain the time and frequency domain signals for the mechanical mode. PD: photodetector; OSC: oscilloscope; ESA: Electrical spectrum analyzer.

with an oscilloscope in order to monitor the time-domain behavior, and also with an Electrical Spectrum Analyzer (ESA) to obtain the power spectra.

II.   BIFURCATION IN THE VICINITY OF THE EXCEPTIONAL POINT

For the compound phonon laser system considered in this work, there exists an exceptional point for the optical modes in the coupled resonators and a bifurcation occurs in the vicinity of this exceptional point. In fact, the coupling between the two optical modes a_1 and a_2 in the two resonators with strength κ gives rise to two optical supermodes $a_\pm$ with complex eigenfrequencies $\omega_\pm = \Delta\omega - i\chi \pm \beta$ (in a frame rotating with ω_p) where $\Delta\omega = \omega_0 - \omega_p$ is the detuning between the optical pump frequency ω_p and the cavity resonance frequency ω_0, $\chi = (\gamma_1 + \gamma_2)/2$, $\beta = \sqrt{\kappa^2 - \gamma^2}$, and $\gamma = (\gamma_2 - \gamma_1)/2$. $\gamma_1 = \gamma_{10} + \gamma_{c1}$ and $\gamma_2 = \gamma_{20} + \gamma_{tip}$ represent the damping rates of a_1 and a_2. γ_{10} and γ_{20} are the intrinsic damping rates of a_1 and a_2 induced e.g. by the material absorption, scattering, and radiation losses. γ_{c1} is the damping rate of a_1 induced by the coupling between the resonator and the fiber-taper and γ_{tip} is the additional loss induced by the nanotip. When $\gamma < \kappa$, the two supermodes are non-degenerate with frequencies $\Delta\omega \pm \beta$ and the same damping rate χ (see Fig. S2a and Fig. S2b). This case is referred to as the regime before the exceptional point. On the other hand, when $\gamma > \kappa$, the two supermodes are degenerate with frequency $\Delta\omega$ but different damping rates $\chi \pm i\beta$ (see Fig. S2a and Fig. S2b), which is referred to as the regime after the exceptional point. At $\kappa = \gamma$, i.e., at the exceptional point, the two supermodes are degenerate with equal damping rate, indicating a transition between the regime before the exceptional point and the regime after the exceptional point. In Fig. S2c-S2e we show the output spectra of the optical supermodes which exhibit the degeneracy of the optical modes at the exceptional point.
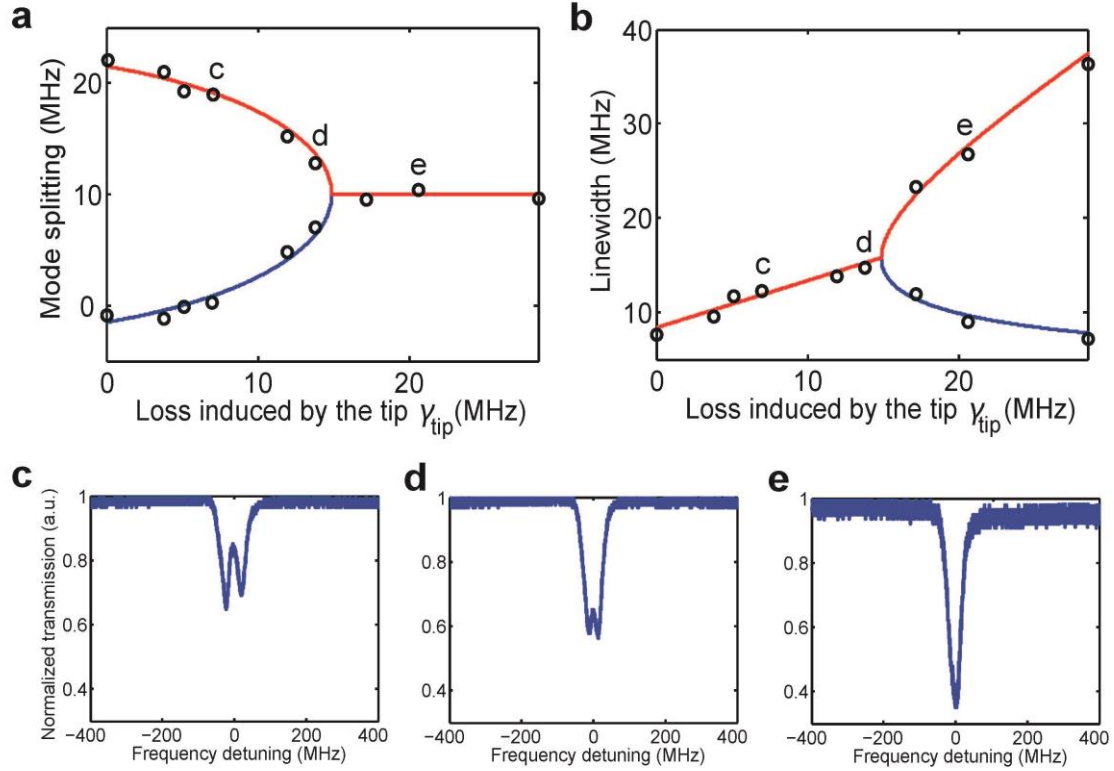
Figure S2. Bifurcation in the vicinity of the exceptional point in the compound phonon laser system. a, Real part of the eigenfrequencies of the optical supermodes as a function of the loss induced by the nanotip γ_{tip}, which shows the mode splitting and coalescence in the vicinity of the exceptional point. **b**, Imaginary part of the eigenfrequencies of the optical supermodes as a function of the loss induced by the nanotip γ_{tip}, which illustrates the linewidth bifurcation of the optical supermodes. **c-e**, Output spectra of the optical supermodes (c) before the exceptional point, which features mode splitting, (d) in the vicinity of the exceptional point, which shows overlapping optical supermodes with equal linewidths, and (e) after the exceptional point, where the optical supermodes are overlapping with different linewidths. Note that only the high-Q supermode, which is localized in the high-Q resonator in the regime after the exceptional point, can be seen in the output spectrum, the parameters for the low-Q supermode can be estimated indirectly from the theoretical model and those of the high-Q mode.

III.   THRESHOLD OF THE PHONON LASER

To understand the physical mechanism behind the phonon laser, let us compare it with the one-dimesional cavity-mediated optical laser system shown in Fig. S3a, which is composed of an optical cavity with one fully-reflecting mirror at one end and a partially-reflecting mirror at the other end. The input pump field leads to the population inversion of the gain medium uniformly distributed in the cavity, and coherent photons are generated by the stimulated emission process which leads to the laser output. Figure S3b shows a picture of the lasing process in which coherent photons are generated by the interaction between the optical mode and the effective two-level atoms in the gain medium. The phonon laser in our system is somewhat similar to this picture of an optical laser to the extent that two optical supermodes act as a two-level system interacting with the phonon field. The mechanical mode supported by the microtoroid resonator interacts with the analog "two-level system" generated by the optical supermodes to receive phonon gain, and then suffers loss during transmission (see Fig. S3c and Fig. S3d). The balance between mechanical gain and mechanical loss leads to the phonon laser demonstrated in the experiments. Due to the similarity between the working principle of a phonon laser and that of an optical laser, one can derive the expressions for the threshold and the linewidth of the phonon laser following the approach carried out for an optical laser.
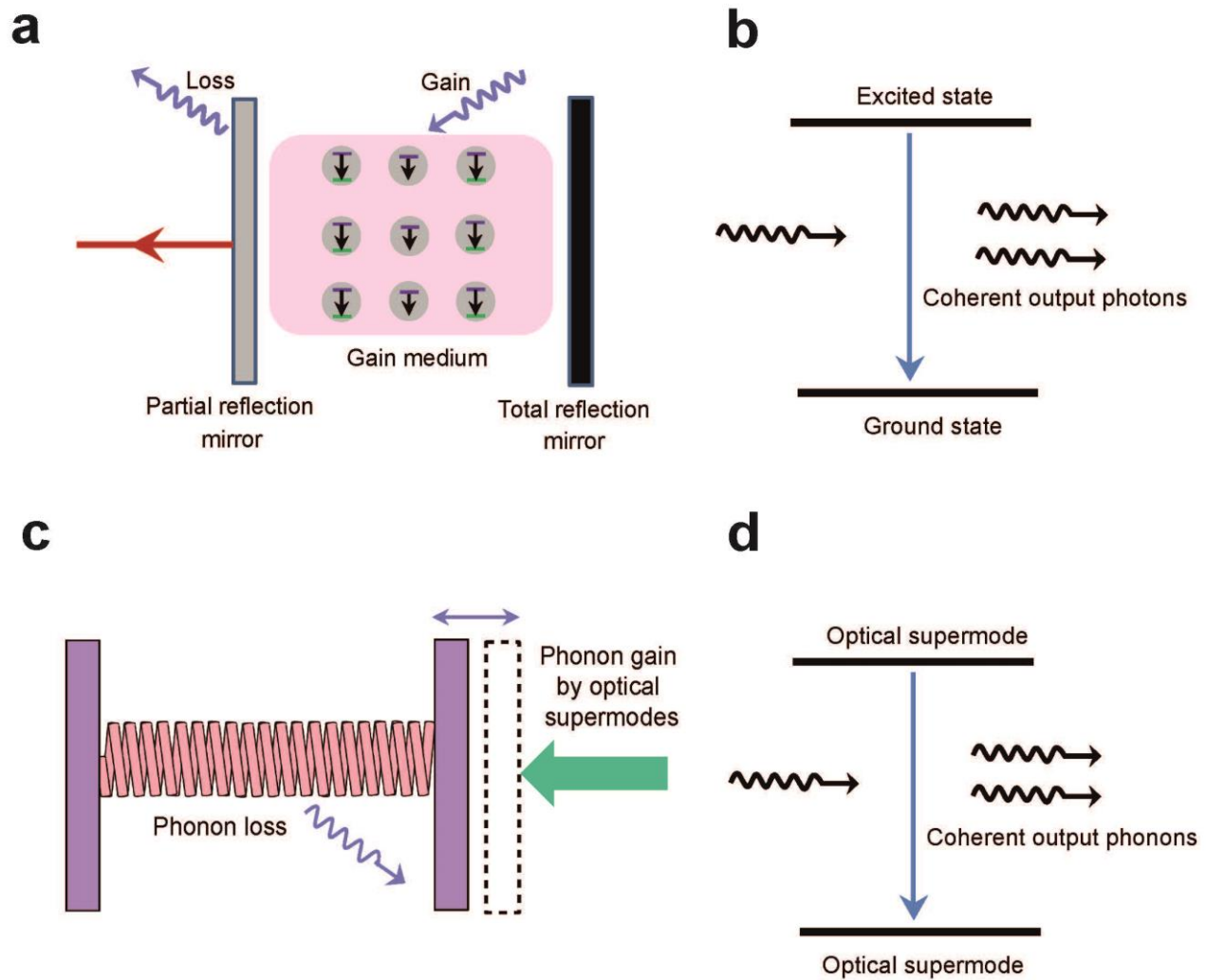
Figure S3. Comparison of an optical laser and a phonon laser. a, Diagram of a one-dimensional optical laser with a gain medium distributed in an optical cavity with one fully-reflecting mirror at one end and a patially-reflecting mirror at the other end. **b**, Mechanism of an optical laser, in which an optical mode interacts with a gain medium and coherent output photons are generated. **c**, Equivalent one-dimensional phonon laser with gain provided by the optical supermodes acting as a "two-level system". **d**, Equivalent mechanism of the phonon laser in which the mechanical mode interacts with the analog two-level system represented by the optical supermodes such that coherent output phonons are generated.

In the following, we perform the derivation of the threshold of the phonon laser. Denoting the intracavity fields of the two resonators as a_1 and a_2 in a frame rotating with the frequency of the driving field, and the phonon mode as b, the dynamical equations for our system can be written as

$$\frac{d}{dt}a_1 = \left[-\gamma_1 + i\left(\omega_p - \omega_1\right)\right]a_1 - i\kappa a_2 - ig_{om}a_1\left(b + b^*\right) + \sqrt{2\gamma_{c1}}\varepsilon, \tag{S.1}$$

$$\frac{d}{dt}a_2 = -i\kappa a_1 + \left[-\gamma_2 + i\left(\omega_p - \omega_2\right)\right]a_2, \tag{S.2}$$

$$\frac{d}{dt}b = -\left(\Gamma_m + i\Omega_m\right)b - ig_{om}a_1^*a_1, \tag{S.3}$$

where ω_1 and ω_2 are the cavity-mode line center frequencies of a_1 and a_2, ω_p is the frequency of the driving field, g_{om} is the optomechanical coupling strength, and ε is the amplitude of the input field fed into the first resonator. $\gamma_1 = \gamma_{10} + \gamma_{c1}$ and $\gamma_2 = \gamma_{20} + \gamma_{tip}$ represent the damping rates of a_1 and a_2, in which γ_{10} and γ_{20} are the intrinsic damping rates of a_1 and a_2, γ_{c1} is the damping rate of a_1 induced by the coupling between the resonator and the fiber-taper, and γ_{tip} is the additional loss induced by the nanotip. Ω_m and Γ_m are the frequency and damping rate of the mechanical mode. The two optical fields a_1 and a_2 couple to each other via the evanescent field with coupling strength κ, which gives rise to two optical supermodes

$$\begin{pmatrix} a_+ \\ a_- \end{pmatrix} = \begin{pmatrix} \mathcal{N}_-^{-1} & \\ & \mathcal{N}_+^{-1} \end{pmatrix}\begin{pmatrix} \tau_+ & \tau_- \\ 1 & 1 \end{pmatrix}^{-1}\begin{pmatrix} a_1 \\ a_2 \end{pmatrix} = \begin{pmatrix} \mathcal{N}_-^{-1} & \\ & \mathcal{N}_+^{-1} \end{pmatrix}\begin{pmatrix} \mu & -\lambda_- \\ -\mu & \lambda_+ \end{pmatrix}\begin{pmatrix} a_1 \\ a_2 \end{pmatrix} \tag{S.4}$$

with complex eigenfrequencies

$$\omega_\pm = -\Delta_+ - i\chi \pm \sqrt{\kappa^2 + \left(\Delta_- + i\gamma\right)^2}, \tag{S.5}$$

where $\chi = (\gamma_1 + \gamma_2)/2$, $\beta + i\tilde{\beta} = \sqrt{\kappa^2 - \gamma^2}$, $\gamma = (\gamma_2 - \gamma_1)/2$, $\Delta_\pm = \left[(\omega_p - \omega_1) \pm (\omega_p - \omega_2)\right]/2$, and

$$\tau_\pm = \frac{\Delta_- + i\gamma}{\kappa} \pm \sqrt{1 + \left(\frac{\Delta_- + i\gamma}{\kappa}\right)^2},$$

$$\mu = \frac{1}{\tau_+ - \tau_-} = \frac{\kappa}{2\left[\kappa^2 + (\Delta_- + i\gamma)^2\right]^{1/2}},$$

$$\lambda_\pm = \frac{\tau_\pm}{\tau_+ - \tau_-} = \frac{\Delta_- + i\gamma \pm \left[\kappa^2 + (\Delta_- + i\gamma)^2\right]^{1/2}}{2\left[\kappa^2 + (\Delta_- + i\gamma)^2\right]^{1/2}}. \tag{S.6}$$

$\mathcal{N}_\pm$ are normalization constants which are given by

$$\mathcal{N}_\pm = \sqrt{|\mu|^2 + |\lambda_\pm|^2}.$$

Note that we have omitted the influence of the nonlinear optomechanical coupling for writing down the expressions for the optical supermodes under the assumption that the optomechanical coupling strength is weak, which has been widely used in the existing phonon laser literature [S1]-[S5]. For the case with strong optomechanical coupling, the mechanical mode would induce additional detuning and thus shift the optical supermodes [S6] which is not considered in our discussions. Since the physical phenomena that we are interested in appear in the regime where the system is in the vicinity of the exceptional point, we will mainly focus on this regime in the following discussions.

a. The regime before the exceptional point $\gamma \leq \kappa$

Let us first consider the regime before the exceptional point in which $\beta \neq 0$, $\tilde{\beta} = 0$ and assume that the intracavity resonance frequencies of the two resonators are degenerate, i.e. $\omega_1 = \omega_2 \triangleq \omega_0$. In this case, the two optical supermodes can be simplified according to

$$\begin{pmatrix} a_+ \\ a_- \end{pmatrix} = \frac{\sqrt{2}\beta}{\kappa} \begin{pmatrix} (\beta+i\gamma)/\kappa & (-\beta+i\gamma)/\kappa \\ 1 & 1 \end{pmatrix}^{-1} \begin{pmatrix} a_1 \\ a_2 \end{pmatrix}$$

$$= \frac{\sqrt{2}\beta}{\kappa} \begin{pmatrix} \mu & -\lambda_- \\ -\mu & \lambda_+ \end{pmatrix} \begin{pmatrix} a_1 \\ a_2 \end{pmatrix} \quad (S.7)$$

with complex eigenfrequencies

$$\omega_\pm = \omega_0 - \omega_p \pm \beta - i\chi, \quad (S.8)$$

where

$$\mu = \frac{\kappa}{2\beta}, \quad \lambda_\pm = \frac{i\gamma \pm \beta}{2\beta}. \quad (S.9)$$

If we omit the self-frequency-shift terms $a_+^* a_+ (b+b^*)$ and $a_-^* a_- (b+b^*)$ and non-resonant terms like

$a_-^* a_+ b$ and $a_+^* a_- b^*$ in the Hamiltonian of the optomechanical coupling, the dynamical equations for the

optical supermodes $a_\pm$ can be expressed as [S1], [S2]

$$\frac{d}{dt} a_- = -\left[\chi + i(\omega_0 - \omega_p - \beta)\right] a_- + i g_{om} \frac{i\gamma - \beta}{2\beta} a_+ b^* + \sqrt{2\gamma_{c1}} \tilde{\varepsilon}, \quad (S.10)$$

$$\frac{d}{dt} a_+ = -\left[\chi + i(\omega_0 - \omega_p + \beta)\right] a_+ - i g_{om} \frac{i\gamma + \beta}{2\beta} a_- b - \sqrt{2\gamma_{c1}} \tilde{\varepsilon}, \quad (S.11)$$

$$\frac{d}{dt} b = -(\Gamma_m + i\Omega_m) b - i g_{om} \frac{(\gamma + i\beta)^2}{2\beta^2} a_-^* a_+, \quad (S.12)$$

where $\tilde{\varepsilon} = \left(\sqrt{2}\beta\mu\varepsilon\right)/\kappa = \varepsilon/\sqrt{2}$. Note that here we have omitted the anti-Stokes mode which is out of the

frequency bands of the two optical supermodes $a_\pm$.

The optical supermodes a_+ and a_- mimic a two-level system where the transitions between the energy

levels are mediated by the mechanical mode, which gives rise to the phonon laser. To illustrate this, we

define the ladder operators and population inversion quantities by the optical modes a_+ and a_- as

$$J_+ = a_+^* a_-, \quad J_- = a_-^* a_+, \quad J_z = a_+^* a_+ - a_-^* a_-, \quad (S.13)$$

From Eqs. (S.10)-(S.12) and taking the stationary states of the supermodes in the driving terms acting on the "two-level system", we have [S1], [S2]

$$\dot{J}_- = -2\left(\chi + i\beta\right)J_- + i\tilde{g}_{om}bJ_z,$$
(S.14)

$$\dot{J}_+ = -2\left(\chi - i\beta\right)J_+ - i\tilde{g}_{om}^* b^* J_z,$$
(S.15)

$$\dot{J}_z = -2\chi J_z + 2i\tilde{g}_{om}^* b^* J_- - 2i\tilde{g}_{om}bJ_+ + \Lambda,$$
(S.16)

$$\dot{b} = -\left(\Gamma_m + i\Omega_m\right)b - ig_{om}\frac{\left(\gamma + i\beta\right)^2}{2\beta^2}J_-.$$
(S.17)

$\tilde{g}_{om}$ denotes the effective optomechanical coupling strength in the supermode picture given by

$$\tilde{g}_{om} = g_{om}\frac{i\gamma + \beta}{2\beta},$$
(S.18)

which already takes very large values in the vicinity of an exceptional point (i.e., very small non-zero values of β). While this observation implies EP-enhanced optomechanical interaction, the divergence of (S.18) directly at the EP ($\beta = 0$) also indicates that more terms are required to describe this parameter regime correctly. Λ is the effective pumping acting on the two-level system which can be expressed as

$$\Lambda = \sqrt{2\gamma_{c1}}\left(\tilde{\varepsilon}^* a_{ss,+} + a_{ss,+}^*\tilde{\varepsilon} + \tilde{\varepsilon}^* a_{ss,-} + a_{ss,-}^*\tilde{\varepsilon}\right),$$
(S.19)

where $a_{ss,+}$ and $a_{ss,-}$ are the stationary values of the supermodes $a_\pm$ from Eqs. (S.10) and (S.11). The factor 2 in the denominator of Eq. (S.18) comes from the fact that g_{om} is defined as the optomechanical coupling strength in the solitary resonator (i.e., single travelling mode in the resonator with mechanical mode) while $\tilde{g}_{om}$ in Eq. (S.18) is defined for the supermodes formed in the coupled resonators system.

Note that here we have omitted the driving terms acting on the dynamics of J_- and J_+ since we assume that the total population distribution of the two energy levels $n_+ + n_- = a_+^* a_+ + a_-^* a_-$ is conserved, an

approximation which has already been introduced in previous phonon laser papers [S1]-[S5]. Transferring the variables to the rotating frame by setting $\tilde{b} = \exp(i\Omega_m t) b$, $\tilde{J}_- = \exp(i\Omega_m t) J_-$, and $\tilde{J}_+ = \exp(-i\Omega_m t) J_+$, Eqs. (S.14)-(S.17) can be rewritten as

$$\dot{\tilde{J}}_- = -2\left[\chi - i\left(\Omega_m/2 - \beta\right)\right]\tilde{J}_- + i\tilde{g}_{om}J_z\tilde{b}, \tag{S.20}$$

$$\dot{\tilde{J}}_+ = -2\left[\chi + i\left(\Omega_m/2 - \beta\right)\right]\tilde{J}_+ - i\tilde{g}_{om}^*\tilde{b}^*J_z, \tag{S.21}$$

$$\dot{J}_z = -2\chi J_z + 2i\tilde{g}_{om}^*\tilde{b}^*\tilde{J}_- - 2i\tilde{g}_{om}\tilde{b}\tilde{J}_+ + \Lambda, \tag{S.22}$$

$$\dot{\tilde{b}} = -\Gamma_m\tilde{b} - ig_{om}\frac{(\gamma + i\beta)^2}{2\beta^2}\tilde{J}_-. \tag{S.23}$$

We can adiabatically eliminate the degrees of freedom of the optical modes by setting $\dot{\tilde{J}}_- = 0$ due to the reason that $\Gamma_m \ll \chi$, by which we obtain

$$\tilde{J}_- = \frac{i\tilde{g}_{om}J_z}{2\left[\chi - i\left(\Omega_m/2 - \beta\right)\right]}\tilde{b} = \frac{g_{om}J_z\left(-\gamma + i\beta\right)/(2\beta)}{2\left[\chi - i\left(\Omega_m/2 - \beta\right)\right]}\tilde{b}. \tag{S.24}$$

Substituting Eq. (S.18) and Eq. (S.24) into Eq. (S.23) yields

$$\dot{\tilde{b}} = -\left\{\Gamma_m - \frac{-ig_{om}^2(\gamma + i\beta)\kappa^2 J_z}{8\beta^3\left[\chi - i\left(\Omega_m/2 - \beta\right)\right]}\right\}\tilde{b}. \tag{S.25}$$

One finds that the optical modes induce an effective mechanical gain of

$$G = \mathrm{Re}\left\{\frac{-ig_{om}^2(\gamma + i\beta)\kappa^2 J_z}{8\beta^3\left[\chi - i\left(\Omega_m/2 - \beta\right)\right]}\right\} = \frac{g_{om}^2\kappa^2\left[\beta\chi + \gamma\left(\Omega_m/2 - \beta\right)\right]J_z}{8\beta^3\left[\chi^2 + \left(\Omega_m/2 - \beta\right)^2\right]}. \tag{S.26}$$

By setting $\Gamma_m = G$, we obtain the threshold of the phonon laser in the regime before the exceptional point

$$P_{\mathrm{threshold}} = \chi\hbar\tilde{\omega}_+ a_+^* a_+ \approx \chi\hbar\tilde{\omega}_+ J_z \approx \frac{8\hbar\Gamma_m\beta^3\chi\left[\chi^2 + \left(\Omega_m/2 - \beta\right)^2\right]\tilde{\omega}_+}{g_{om}^2\kappa^2\left[\beta\chi + \gamma\left(\Omega_m/2 - \beta\right)\right]}, \tag{S.27}$$

where $\tilde{\omega}_+$ is the central frequency of a_+. Here, we have assumed that the phonon laser satisfies the condition of complete inversion such that $N_+ = a_+^* a_+ \approx J_z = a_+^* a_+ - a_-^* a_-$. Considering that $\tilde{\omega}_+ = \omega_0 + \beta \approx \omega_0$, equation (S.27) can be rewritten as

$$P_{\text{threshold}} = \frac{8\hbar\Gamma_m \beta^3 \chi \left[\chi^2 + \left(\Omega_m/2 - \beta\right)^2 \right]\omega_0}{g_{om}^2 \kappa^2 \left[\beta\chi + \gamma\left(\Omega_m/2 - \beta\right) \right]}. \tag{S.28}$$

Let us now take a look on two different limiting cases. First, we consider the situation when the system is far away from the exceptional point such that $2\beta \gg \chi$ and $\kappa \gg \gamma$. In this case, the threshold power given by Eq. (S.28) can be expressed as

$$P_{\text{threshold}} = \frac{8\hbar\Gamma_m \kappa\chi \left[\chi^2 + \left(\Omega_m/2 - \kappa\right)^2 \right]\omega_0}{g_{om}^2}. \tag{S.29}$$

Let us then consider the opposite situation in which the system is in the vicinity of the exceptional point such that $\beta \ll \Omega_m/2$, $\left(\Omega_m\gamma\right)/\left(2\chi\right)$ and $\kappa \approx \gamma$. In this case, equation (S.28) can be simplified to

$$P_{\text{threshold}} = \frac{16\hbar\Gamma_m \beta^3 \chi \left[\chi^2 + \left(\Omega_m/2\right)^2 \right]\omega_0}{\kappa^3 g_{om}^2 \Omega_m}. \tag{S.30}$$

It can be seen from Eq. (S.30) that the phonon laser features a very low threshold in the vicinity of the exceptional point, where $\kappa \approx \gamma$ or equivalently $\beta \approx 0$.
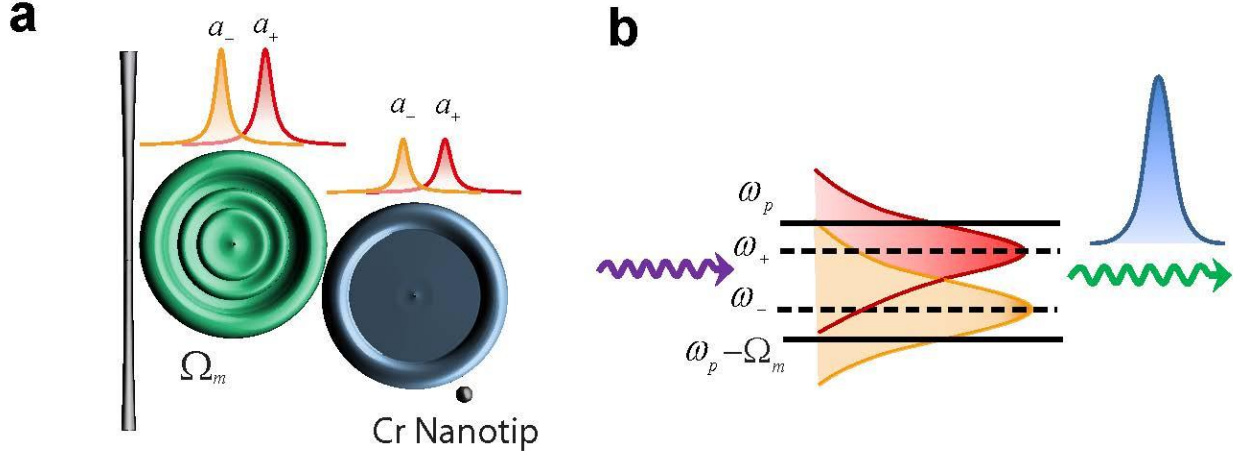
Figure S4. Mechanism of the phonon laser in the regime before the exceptional point. a, Energy distribution of the optical supermodes $a_{\pm}$ in the two resonators: the optical supermodes $a_{\pm}$ are almost equally distributed in the left and right resonators. **b,** Distribution of the pump mode and the Stokes mode that stimulate the phonon laser: the pump mode and the Stokes mode are within the frequency bands of the two optical supermodes $a_{\pm}$.

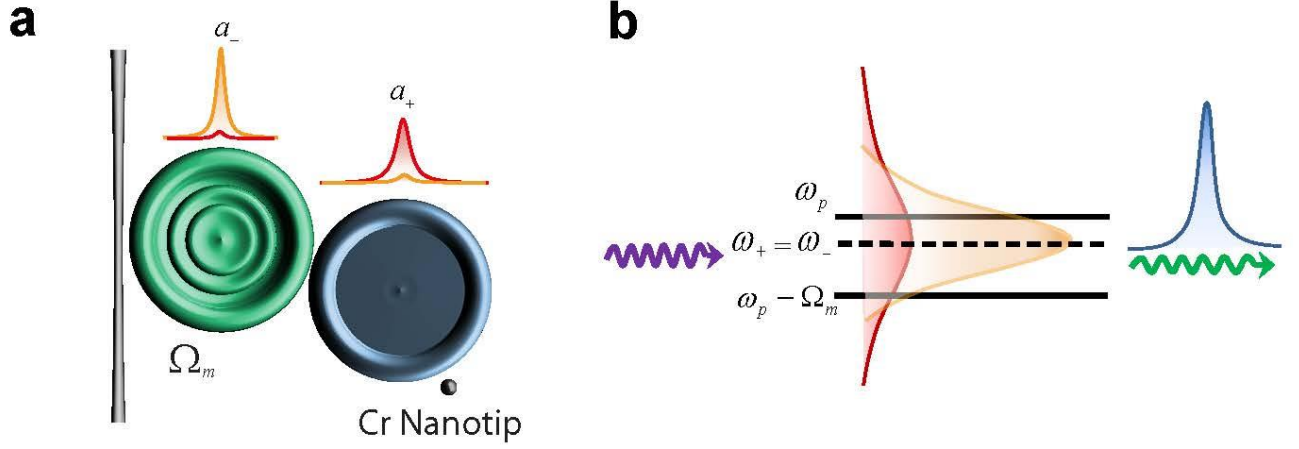### b. The regime after the exceptional point $\gamma > \kappa$

In the regime after the exceptional point where $\beta = 0$, $\tilde{\beta} \neq 0$, the supermodes of the two-coupled resonators are frequency-degenerate but have different effective damping rates. The high-Q (low-Q) supermode is mainly localized in the microresonator without (with) the Cr-tip. In the vicinity of the exceptional point, the dynamical equations of the system in this regime are then given by

$$\frac{d}{dt}a_- = -\left[(\chi - \tilde{\beta}) + i(\omega_0 - \omega_p) \right]a_- - i\frac{\gamma + \tilde{\beta}}{2\tilde{\beta}} g_{om} a_+ b + \sqrt{2\gamma_{c1}}\tilde{\varepsilon}_-, \tag{S.31}$$

$$\frac{d}{dt}a_+ = -\left[(\chi + \tilde{\beta}) + i(\omega_0 - \omega_p) \right]a_+ + i\frac{\gamma + \tilde{\beta}}{2\tilde{\beta}} g_{om} a_- b^* - \sqrt{2\gamma_{c1}}\tilde{\varepsilon}_+, \tag{S.32}$$

$$\frac{d}{dt}b = -(\Gamma_m + i\Omega_m)b - ig_{om}\frac{(\gamma + \tilde{\beta})^2}{2\tilde{\beta}^2}a_+^* a_-, \tag{S.33}$$

where $\tilde{\beta} = \sqrt{\gamma^2 - \kappa^2}$ and $\tilde{\bar{\varepsilon}}_{\pm} = -i\kappa\varepsilon \big/ \sqrt{2\gamma^2 \pm 2\gamma\tilde{\beta}}$.

Figure S5. Mechanism of the phonon laser in the regime after the exceptional point. a, Energy distribution of the optical supermodes $a_{\pm}$ in the two resonators: the high-Q optical supermode a_{-} is mainly distributed in the left resonator supporting the mechanical mode and the low-Q optical supermode a_{+} is mainly distributed in the right resonator. **b,** Distribution of the pump mode and the Stokes mode that stimulate the phonon laser: the pump mode and the Stokes mode are mainly distributed in the frequency bands of the high-Q optical supermode a_{-} and the low-Q optical supermode a_{+}, which are degenerate.

Similar as before, we redefine the ladder and population inversion operators by the optical modes a_{+} and a_{-} as

$$\overline{J}_{-} = a_{+}^{*}a_{-}, \qquad \overline{J}_{+} = a_{-}^{*}a_{+}, \qquad \overline{J}_{z} = a_{-}^{*}a_{-} - a_{+}^{*}a_{+},$$

and introduce the rotating frame $\tilde{b} = \exp(i\Omega_m t)b$ and $\tilde{\overline{J}}_{-} = \exp(i\Omega_m t)\overline{J}_{-}$, which leads to

$$\dot{\tilde{\overline{J}}}_{-} = -2\left(\chi - i\frac{\Omega_m}{2}\right)\tilde{\overline{J}}_{-} + \frac{ig_{om}\left(\gamma + \tilde{\beta}\right)}{2\tilde{\beta}}\overline{J}_{z}\tilde{b}, \tag{S.34}$$

$$\dot{\tilde{b}} = -\Gamma_m \tilde{b} - ig_{om} \frac{\left(\gamma + \tilde{\beta}\right)^2}{2\tilde{\beta}^2} \tilde{\tilde{J}}_-.$$

(S.35)

Adiabatically eliminating the degrees of freedom of the optical modes by setting $\dot{\tilde{J}}_- = 0$ gives

$$\tilde{\tilde{J}}_- = \frac{i\left(\gamma + \tilde{\beta}\right) g_{om} \bar{J}_z}{4\tilde{\beta}\left(\chi - i\Omega_m/2\right)} \tilde{b},$$

(S.36)

and substituting this result into Eq. (S.35) yields

$$\dot{\tilde{b}} = -\left[\Gamma_m - \frac{\left(\gamma + \tilde{\beta}\right)^3 g_{om}^2 \bar{J}_z}{8\tilde{\beta}^3 \left(\chi - i\Omega_m/2\right)}\right] \tilde{b}.$$

(S.37)

Thus, the optical modes induce an effective mechanical gain

$$G = \frac{\left(\gamma + \tilde{\beta}\right)^3 g_{om}^2 \bar{J}_z \chi}{8\tilde{\beta}^3 \left[\chi^2 + \left(\Omega_m/2\right)^2\right]}.$$

(S.38)

By setting $\Gamma_m = G$, we obtain the threshold of the phonon laser in the regime after the exceptional point,

$$\tilde{P}_{\text{threshold}} = \left(\chi - \tilde{\beta}\right)\hbar\omega_0 \bar{J}_z = \frac{8\hbar\Gamma_m \left(\chi - \tilde{\beta}\right)\tilde{\beta}^3 \left[\chi^2 + \left(\Omega_m/2\right)^2\right]\omega_0}{g_{om}^2 \chi\left(\gamma + \tilde{\beta}\right)^3}.$$

(S.39)

Similar to the regime before the exceptional point, we want to consider two different limiting cases. First, we treat the situation when the system is far away from the exceptional point such that $\gamma \gg \kappa$. Under these circumstances, the threshold power given by Eq. (S.39) can be expressed as

$$\tilde{P}_{\text{threshold}} = \frac{8\hbar\Gamma_m \left(\chi - \gamma\right)\left[\chi^2 + \left(\Omega_m/2\right)^2\right]\omega_0}{g_{om}^2 \chi}.$$

(S.40)

Let us then consider the opposite case in which the system is in the vicinity of the exceptional point such that $\kappa \approx \gamma$. In this case, we have $\chi \gg \tilde{\beta}$, and Eq. (S.39) can be expressed as

$$\tilde{P}_{\text{threshold}} \approx \frac{8\hbar\Gamma_m\tilde{\beta}^3\left[\chi^2+\left(\Omega_m/2\right)^2\right]\omega_0}{g_{om}^2\gamma^3}, \tag{S.41}$$

which is extremely low in the vicinity of the exceptional point where $\tilde{\beta} \approx 0$.

Employing the system parameters $\Omega_m=17.38$ MHz, $g_{om}=1.5$ kHz, $\Gamma_m=40$ kHz, $\gamma_1=3.16$ MHz, $\gamma_2=13.56$ MHz, we plot the curve of the phonon laser threshold versus the tip-induced loss rate γ_{tip} for
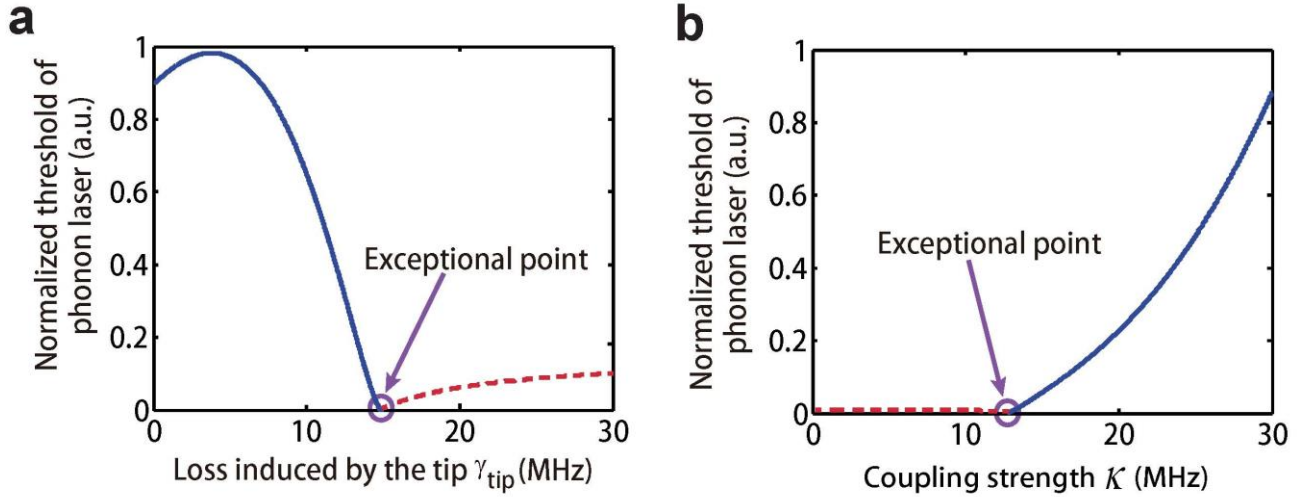
Figure S6. Threshold of the phonon laser $P_{\text{threshold}}$ in the vicinity of the exceptional point. a, $P_{\text{threshold}}$ versus the tip-induced damping rate γ_{tip}. $P_{\text{threshold}}$ first increases with the increase of γ_{tip}, reaches a maximal value, and then decreases with increasing γ_{tip}. Around the exceptional point, there is a sudden drop of $P_{\text{threshold}}$ which represents the transition. **b,** $P_{\text{threshold}}$ versus the coupling strength κ. $P_{\text{threshold}}$ remains to be very small when κ is small and then after the exceptional point, it increases with growing κ. Blue and red curves are obtained using Eqs. (S.30) and (S.41) respectively. The circled points represent the exceptional point where we have $\beta=0$ and $\tilde{\beta}=0$ and Eqs. (S.30) and (S.41) become equal.

fixed coupling strength $\kappa = 12.63$ MHz in Fig. S6a and the phonon laser threshold versus the coupling

strength κ for fixed $\gamma_{tip} = 15$ MHz in Fig. S6b. The threshold of the phonon laser is given by Eq. (S.28)

and Eq. (S.39). The numerical results in Fig. S6a show a drop of the threshold of the phonon laser in the

vicinity of the exceptional point which fits very well with our analysis and the experimental results.

IV. LINEWIDTH OF THE PHONON LASER

a. The regime before the exceptional point $\gamma \leq \kappa$

In order to calculate the linewidth of the phonon laser, we have to reconsider the system dynamics by

introducing fluctuation terms. In this way, the dynamical equations (S.20)-(S.23) are written as

$$\dot{\tilde{J}}_- = -2\left[\chi - i\left(\Omega_m/2 - \beta\right)\right]\tilde{J}_- + g_{om}\frac{-\gamma + i\beta}{2\beta}J_z\tilde{b} + \xi_-(t), \tag{S.42}$$

$$\dot{\tilde{J}}_+ = -2\left[\chi + i\left(\Omega_m/2 - \beta\right)\right]\tilde{J}_+ + g_{om}\frac{-\gamma - i\beta}{2\beta}\tilde{b}^*J_z + \xi_-^*(t), \tag{S.43}$$

$$\dot{J}_z = -2\chi J_z + g_{om}\frac{\gamma + i\beta}{\beta}\tilde{b}^*\tilde{J}_- + g_{om}\frac{\gamma - i\beta}{\beta}\tilde{b}\tilde{J}_+ + \Lambda + \xi_z(t), \tag{S.44}$$

$$\dot{\tilde{b}} = -\Gamma_m\tilde{b} - ig_{om}\frac{(\gamma + i\beta)^2}{2\beta^2}\tilde{J}_- + \xi_b(t), \tag{S.45}$$

where the noise terms $\xi_-(t), \xi_z(t), \xi_b(t)$ are assumed to be white noises such that [S7]

$$\left\langle\xi_-(t)\xi_-^\dagger(t')\right\rangle = 2\chi\delta(t - t'), \quad \left\langle\xi_-^\dagger(t)\xi_-(t')\right\rangle = 0,$$

$$\left\langle\xi_z(t)\xi_z(t')\right\rangle = 2\chi\delta(t - t'), \tag{S.46}$$

$$\left\langle\xi_b(t)\xi_b^\dagger(t')\right\rangle = 2\Gamma_m(n_{bT} + 1)\delta(t - t'), \quad \left\langle\xi_b^\dagger(t)\xi_b(t')\right\rangle = 2\Gamma_m n_{bT}\delta(t - t').$$

n_{bT} denotes the mean phonon number of the phonon bath in thermal equilibrium. By letting $\dot{\tilde{J}}_- = 0$ and

$\dot{\tilde{J}}_+ = 0$ to adiabatically eliminate the degrees of freedom of $\tilde{J}_-$ and $\tilde{J}_+$, we find the following equations

for J_z and $\tilde{b}$,

$$\dot{J}_z = -2\chi \left\{ 1 + \frac{g_{om}^2 \kappa^2}{4\left[\chi^2 + \left(\Omega_m/2 - \beta\right)^2 \right]\beta^2} n_b \right\} J_z + \Lambda + \tilde{\xi}_z(t),$$

(S.47)

$$\dot{\tilde{b}} = -\left\{ \Gamma_m - \frac{ig_{om}^2 \kappa^2 \left(\gamma + i\beta\right)}{8\beta^3 \left[\chi - i\left(\Omega_m/2 - \beta\right) \right]} J_z \right\} \tilde{b} + \tilde{\xi}_b(t),$$

(S.48)

where $\tilde{\xi}_z(t)$ and $\tilde{\xi}_b(t)$ are effective fluctuation terms which are given by

$$\tilde{\xi}_z(t) = \xi_z(t) + \frac{ig_{om}\left[\left(\beta - i\gamma\right)/\beta \right]}{2\chi - 2i\left(\Omega_m/2 - \beta\right)} b_{ss}^* \xi_-(t) + \frac{-ig_{om}\left[\left(\beta + i\gamma\right)/\beta \right]}{2\chi + 2i\left(\Omega_m/2 - \beta\right)} b_{ss} \xi_-^*(t),$$

(S.49)

$$\tilde{\xi}_b(t) = \xi_b(t) + \frac{-ig_{om}\left(\gamma + i\beta\right)^2}{4\left[\chi - i\left(\Omega_m/2 - \beta\right) \right]\beta^2} \xi_-(t),$$

(S.50)

and $b_{ss} = \sqrt{n_{b,ss}}\, e^{i\phi_{ss}}$ is the stationary value of the phonon field with $\sqrt{n_{b,ss}}$ and ϕ_{ss} respectively being the stationary amplitude and phase of the phonon field. The phonon mode $\tilde{b}$ can be written as

$$\tilde{b} = e^{i\phi_{ss} + i\theta(t)} \left[\sqrt{n_{b,ss}} + \rho(t) \right],$$

(S.51)

where $\theta(t)$ and $\rho(t)$ are respectively the phase and amplitude fluctuations of the phonon field. Assuming that the fluctuation terms are small, we have

$$\tilde{b} \approx e^{i\phi_{ss}} \left[1 + i\theta(t) \right] \left[\sqrt{n_{b,ss}} + \rho(t) \right] \approx \sqrt{n_{b,ss}}\, e^{i\phi_{ss}} + e^{i\phi_{ss}} \left[\rho(t) + i\sqrt{n_{b,ss}}\,\theta(t) \right].$$

(S.52)

The population inversion J_z can be expressed as the sum of its stationary value and a fluctuation term according to

$$J_z = \frac{8\Gamma_m \beta^3 \left[\chi^2 + \left(\Omega_m/2 - \beta\right)^2 \right]}{g_{om}^2 \kappa^2 \left[\gamma\left(\beta - \Omega_m/2\right) + \chi\beta \right]} + \delta J_z.$$

(S.53)

By inserting Eqs. (S.52) and (S.53) into Eq. (S.48), we get

$$\dot{\rho}+i\sqrt{n_{b,ss}}\,\dot{\theta}=e^{-i\phi_{ss}}\dot{\tilde{b}}=\frac{ig_{om}^2\kappa^2\left(\gamma+i\beta\right)}{8\beta^3\left[\chi-i\left(\Omega_m/2-\beta\right)\right]}\sqrt{n_{b,ss}}\,\delta J_z+e^{-i\phi_{ss}}\tilde{\xi}_b\left(t\right),\tag{S.54}$$

and therefore

$$\dot{\rho}=\frac{g_{om}^2\kappa^2\left[\left(\beta-\Omega_m/2\right)\gamma-\beta\chi\right]}{8\left[\chi^2+\left(\Omega_m/2-\beta\right)^2\right]\beta^3}\sqrt{n_{b,ss}}\,\delta J_z+\xi_\rho\left(t\right),\tag{S.55}$$

$$\dot{\theta}=\frac{\left[\chi\gamma+\beta\left(\beta-\Omega_m/2\right)\right]g_{om}^2\kappa^2}{8\left[\chi^2+\left(\Omega_m/2-\beta\right)^2\right]\beta^3}\delta J_z+\xi_\theta\left(t\right),\tag{S.56}$$

in which the fluctuation terms $\xi_\rho\left(t\right)$ and $\xi_\theta\left(t\right)$ are given by

$$\xi_\rho\left(t\right)=\frac{1}{2}\left[e^{-i\phi_{ss}}\tilde{\xi}_b\left(t\right)+e^{i\phi_{ss}}\tilde{\xi}_b^{\dagger}\left(t\right)\right],\tag{S.57}$$

$$\xi_\theta\left(t\right)=\frac{1}{2i\sqrt{n_{b,ss}}}\left[e^{-i\phi_{ss}}\tilde{\xi}_b\left(t\right)-e^{i\phi_{ss}}\tilde{\xi}_b^{\dagger}\left(t\right)\right].\tag{S.58}$$

In order to simplify our discussion, we consider the case when $\beta\ll\Omega_m/2,\chi,\gamma$, which is fulfilled in the vicinity of the exceptional point. Thus, we can obtain the following approximate equation by substituting Eq. (S.53) into Eq. (S.47)

$$\begin{aligned}\delta\dot{J}_z&=-2\chi\left\{1+\frac{g_{om}^2\kappa^2}{4\left[\chi^2+\left(\Omega_m/2-\beta\right)^2\right]\beta^2}\left(n_{b,ss}+2\sqrt{n_{b,ss}}\rho\left(t\right)\right)\right\}\\&\quad\left\{\frac{8\Gamma_m\beta^3\left[\chi^2+\left(\Omega_m/2-\beta\right)^2\right]}{g_{om}^2\kappa^2\left(\beta-\Omega_m/2\right)\gamma}+\delta J_z\right\}+\Lambda+\tilde{\xi}_z\left(t\right)\\&=-2\chi\left\{1+\frac{g_{om}^2\kappa^2}{4\left[\chi^2+\left(\Omega_m/2-\beta\right)^2\right]\beta^2}n_{b,ss}\right\}\delta J_z-\frac{8\beta\chi\Gamma_m}{\gamma\left(\beta-\Omega_m/2\right)}\sqrt{n_{b,ss}}\rho\left(t\right)+\tilde{\xi}_z\left(t\right).\end{aligned}\tag{S.59}$$

Note that we have used the following equation for the stationary state,

$$\Lambda=\frac{16\chi\Gamma_m\left[\chi^2+\left(\Omega_m/2-\beta\right)^2\right]\beta^3}{g_{om}^2\left(\beta-\Omega_m/2\right)\gamma\kappa^2}\left[1+\frac{g_{om}^2\kappa^2}{4\left[\chi^2+\left(\Omega_m/2-\beta\right)^2\right]\beta^2}n_{b,ss}\right].\tag{S.60}$$

Equation (S.59) can be reexpressed as

$$\delta \dot{J}_z = -2\chi\eta\,\delta J_z - \frac{8\beta\chi\Gamma_m}{\gamma(\beta-\Omega_m/2)}\sqrt{n_{b,ss}}\,\rho(t)+\tilde{\xi}_z(t),$$

(S.61)

where

$$\eta = 1+\frac{g_{om}^2\kappa^2}{4\left[\chi^2+(\Omega_m/2-\beta)^2\right]\beta^2}\,n_{b,ss}=\frac{\Lambda}{\Lambda_{th}},$$

(S.62)

and

$$\Lambda_{th}=\frac{16\chi\Gamma_m\left[\chi^2+(\Omega_m/2-\beta)^2\right]\beta^3}{g_{om}^2(\beta-\Omega_m/2)\gamma\kappa^2}$$

(S.63)

is the threshold pump for the phonon laser. By combining Eqs. (S.55), (S.56) and (S.61), we obtain the

following set of equations for the fluctuation terms

$$\dot{\rho}=\frac{g_{om}^2\kappa^2\left[(\beta-\Omega_m/2)\gamma-\beta\chi\right]}{8\left[\chi^2+(\Omega_m/2-\beta)^2\right]\beta^3}\sqrt{n_{b,ss}}\,\delta J_z+\xi_\rho(t),$$

(S.64)

$$\dot{\theta}=\frac{g_{om}^2\kappa^2\left[\chi\gamma+\beta(\beta-\Omega_m/2)\right]}{8\left[\chi^2+(\Omega_m/2-\beta)^2\right]\beta^3}\delta J_z+\xi_\theta(t),$$

(S.65)

$$\delta \dot{J}_z = -2\chi\eta\,\delta J_z - \frac{8\beta\chi\Gamma_m}{\gamma(\beta-\Omega_m/2)}\sqrt{n_{b,ss}}\,\rho(t)+\tilde{\xi}_z(t).$$

(S.66)

The linewidth of the phonon laser is related to the fluctuations of the phase $\theta(t)$. Since we have $g_{om}\ll\chi$,

we can omit the first term at the right side of Eq. (S.65). While this approximation is necessary for the

further calculations, it must be noted, however, that it is not valid in very close vicinity of the EP where

$\beta\approx 0$ and therefore the first term in Eq. (S.65) diverges. With this approximation it follows from Eq.

(S.65) that

$$\dot{\theta}=\xi_\theta(t),$$

(S.67)

which has the formal solution

$$\theta(t) = \int_0^t \xi_\theta(\tau) d\tau,$$ (S.68)

and thus

$$\langle \theta^2(t) \rangle = \int_0^t d\tau' \int_0^t d\tau'' \langle \xi_\theta(\tau') \xi_\theta(\tau'') \rangle$$
$$= \frac{1}{4n_{b,ss}} \int_0^t d\tau' \int_0^t d\tau'' \left[\langle \tilde{\xi}_b(\tau') \tilde{\xi}_b^\dagger(\tau'') \rangle + \langle \tilde{\xi}_b^\dagger(\tau') \tilde{\xi}_b(\tau'') \rangle \right].$$ (S.69)

Recapitulating that

$$\tilde{\xi}_b(t) = \xi_b(t) + \frac{-ig_{om}(\gamma + i\beta)^2}{4\left[\chi - i(\Omega_m/2 - \beta)\right]\beta^2} \xi_-(t),$$ (S.70)

we can write

$$\langle \tilde{\xi}_b(\tau') \tilde{\xi}_b^\dagger(\tau'') \rangle = 2\Gamma_m \left\{ \frac{g_{om}^2 \chi(\kappa^4/\beta^4)}{16\left[\chi^2 + (\Omega_m/2 - \beta)^2\right]\Gamma_m} + (n_{bT} + 1) \right\} \delta(\tau' - \tau''),$$ (S.71)

$$\langle \tilde{\xi}_b^\dagger(\tau'') \tilde{\xi}_b(\tau') \rangle = 2\Gamma_m n_{bT} \delta(\tau' - \tau'').$$ (S.72)

Inserting Eqs. (S.71) and (S.72) into Eq. (S.69) results in

$$\langle \theta^2(t) \rangle = \frac{\Gamma_m}{2n_{b,ss}} \left\{ \frac{g_{om}^2(\kappa^4/\beta^4)\chi}{16\left[\chi^2 + (\Omega_m/2 - \beta)^2\right]\Gamma_m} + (2n_{bT} + 1) \right\} t.$$ (S.73)

By substituting Eqs. (S.68) and (S.73) into Eq. (S.51) and noting that $\theta(t)$ is the integral of its

corresponding noise, we have [S8]

$$\langle \tilde{b} \rangle = \sqrt{n_{b,ss}} e^{i\phi_{ss}} \langle e^{i\theta(t)} \rangle = \sqrt{n_{b,ss}} e^{i\phi_{ss}} e^{-\langle \theta^2(t) \rangle} = \sqrt{n_{b,ss}} e^{i\phi_{ss}} e^{-\frac{\Gamma_m}{2n_{b,ss}} \left\{ \frac{g_{om}^2(\kappa^4/\beta^4)\chi}{16\left[\chi^2 + (\Omega_m/2 - \beta)^2\right]\Gamma_m} + (2n_{bT} + 1) \right\} t},$$ (S.74)

which means that the linewidth of the phonon laser in this regime can be expressed as

$$\Delta \nu = \frac{\Gamma_m}{2n_{b,ss}} \left\{ \frac{g_{om}^2(\kappa^4/\beta^4)\chi}{16\left[\chi^2 + (\Omega_m/2 - \beta)^2\right]\Gamma_m} + (2n_{bT} + 1) \right\}.$$ (S.75)

Additionally, we introduce a phenomenological and power-independent linewidth term $\Delta \nu_0$ in which we pool contributions to the linewidth that are not included in the above model such as those coming from a nonideal population inversion of the medium and from the nonuniformity of the field (as in the case of the optical laser [S9]). Taken together, the linewidth of the phonon laser is then given by

$$\Delta \nu \approx \Delta \nu_0 + \frac{\Gamma_m}{2n_{b,ss}} \left\{ \frac{g_{om}^2 \left(\kappa^4 / \beta^4 \right) \chi}{16 \left[\chi^2 + \left(\Omega_m / 2 - \beta \right)^2 \right] \Gamma_m} + 2n_{bT} + 1 \right\}. \tag{S.76}$$

Using the definition

$$n_{spon} = \frac{g_{om}^2 \left(\kappa^4 / \beta^4 \right) \chi}{32 \left[\chi^2 + \left(\Omega_m / 2 - \beta \right)^2 \right] \Gamma_m}, \tag{S.77}$$

we can write the linewidth as follows

$$\Delta \nu \approx \Delta \nu_0 + \frac{\Gamma_m}{2n_{b,ss}} \left(2n_{spon} + 2n_{bT} + 1 \right). \tag{S.78}$$

With the peak power of the phonon laser P_{peak} being directly proportional to $n_{b,ss}$, this expression shows the same inverse power dependence as in optical laser theory. Analogously to the procedure in optical laser theory [S10], [S11], we have also introduced here the number of spontaneously emitted phonons into the mechanical resonator n_{spon}. In the limit of a perfect match between the frequency difference of the two supermodes and the mechanical resonance frequency, i.e. $2\beta = \Omega_m$, and for equal optical cavity decay rates $\gamma_1 = \gamma_2$, such that $\beta = \kappa$, the expression for n_{spon} simplifies to

$$n_{spon} = \frac{g_{om}^2}{32 \chi \Gamma_m}, \tag{S.79}$$

which is very similar to the already known result from optical laser theory close above the lasing threshold,

$$n_{\text{spon}}^{\text{opt}} = \frac{g^2}{\gamma\Gamma} D_{+,s}, \tag{S.80}$$

in which g represents the coupling between atoms and light, γ the atomic decay rate, Γ the cavity decay rate, and $D_{+,s}$ the saturated occupation of the upper energy level of the two-level system. Using the relation

$$\frac{\gamma\Gamma}{g^2} = D_{+,\text{thr}} - D_{-,\text{thr}}, \tag{S.81}$$

where $D_{+,\text{thr}}$ and $D_{-,\text{thr}}$ are the occupations of the optical supermodes a_+ and a_- at the lasing threshold, the factor n_{spon} can also be expressed by

$$n_{\text{spon}} = \frac{D_{+,s}}{D_{+,\text{thr}} - D_{-,\text{thr}}} \geq 1, \tag{S.82}$$

from which it can be seen that $n_{\text{spon}} \approx 1$ in the case of perfect inversion and close to threshold. Furthermore, we also remark that n_{spon} diverges at an EP occurring in the two-level system, where $D_{+,\text{thr}} = D_{-,\text{thr}}$, and that this divergence can be traced back to the noise term $\xi_-(t)$ in Eq. (S.42), i.e., to the noise in the optical super-modes that provide the gain for the phonon mode. In other words, we can see here how the increased noise in the two-level system directly leads to an increased linewidth in the phonon laser mode.

The difference between the results for our phonon laser given in Eq. (S.79) and for the optical laser given in Eq. (S.80) is a consequence of the different convention for the definitions of β and χ, which causes the factor 32 in the denominator of n_{spon}, as well as of the fact that we have assumed perfect inversion ($D_{+,s} = 1$) for the linewidth derivation above. With the definitions $\beta' \triangleq 2\beta$ and $\chi' \triangleq 2\chi$, Eqs. (S.42)-(S.45) would feature the same structure as the corresponding equations in the optical laser theory [S10], [S11] and we would immediately obtain the result

$$n_{\mathrm{spon}} = \frac{g_{om}^2}{\chi' \Gamma_m}, \tag{S.83}$$

which has exactly the same structure as the corresponding result for the optical laser.

b. The regime after the exceptional point $\gamma > \kappa$

In the regime after the exceptional point, we start from the following dynamical equations including fluctuation terms

$$\dot{\tilde{J}}_- = -2\left(\chi - i\frac{\Omega_m}{2}\right)\tilde{J}_- + \frac{ig_{om}\left(\gamma + \tilde{\beta}\right)}{2\tilde{\beta}}\bar{J}_z\tilde{b} + \xi_-(t), \tag{S.84}$$

$$\dot{\tilde{J}}_+ = -2\left(\chi + i\frac{\Omega_m}{2}\right)\tilde{J}_- - \frac{ig_{om}\left(\gamma + \tilde{\beta}\right)}{2\tilde{\beta}}\bar{J}_z\tilde{b} + \xi_-^*(t), \tag{S.85}$$

$$\dot{\tilde{J}}_z = -2\chi\bar{J}_z - \frac{ig_{om}\left(\gamma + \tilde{\beta}\right)}{\beta}\tilde{b}^*\tilde{J}_- + \frac{ig_{om}\left(\gamma + \tilde{\beta}\right)}{\tilde{\beta}}\tilde{b}\tilde{J}_+ + \Lambda + \xi_z(t), \tag{S.86}$$

$$\dot{\tilde{b}} = -\Gamma_m\tilde{b} - ig_{om}\frac{\left(\gamma + \tilde{\beta}\right)^2}{2\tilde{\beta}^2}\tilde{J}_- + \xi_b(t), \tag{S.87}$$

where $\tilde{\beta} = \sqrt{\gamma^2 - \kappa^2}$ and the fluctuation terms $\xi_-(t), \xi_z(t), \xi_b(t)$ satisfy the conditions written in Eq. (S.46). With similar discussions as before, we can obtain the linewidth equation (S.78) with

$$n_{\mathrm{spon}} = \frac{g_{om}^2\left[\left(\gamma + \tilde{\beta}\right)^4/\tilde{\beta}^4\right]\chi}{32\left[\chi^2 + \left(\Omega_m/2\right)^2\right]\Gamma_m}. \tag{S.88}$$

In the vicinity of the exceptional point, where $\tilde{\beta} \approx 0$, Eq. (S.88) simplifies to

$$n_{\mathrm{spon}} \approx \frac{g_{om}^2\kappa^4\chi}{32\tilde{\beta}^4\left[\chi^2 + \left(\Omega_m/2\right)^2\right]\Gamma_m}. \tag{S.89}$$

Using the system parameters $\Omega_m = 17.38$ MHz, $g_{om} = 1.5$ kHz, $\Gamma_m = 40$ kHz, $\gamma_1 = 3.16$ MHz, $\gamma_2 = 13.56$

MHz, we plot the normalized linewidth of the phonon laser $\left(\Delta v - \Delta v_0\right)/P_{\text{peak}}^{-1}$ versus the tip-induced loss

rate γ_{tip} for fixed coupling strength $\kappa = 12.63$ MHz in Fig. S7a and the normalized linewidth of the

phonon laser versus the coupling strength κ for fixed $\gamma_{\text{tip}} = 15$ MHz in Fig. S7b. The normalized

linewidth of the phonon laser is given by Eq. (S.78) with n_{spon} from Eq. (S.77) in the regime before the

exceptional point and from Eq. (S.88) in the regime after the exceptional point, respectively. Both in the

regime before the EP and in the regime after the EP, the factor n_{spon} is proportional to β^{-4}, which diverges

at the EP and thus leads to an infinite linewidth broadening directly at the EP. We speculate that this

problem of the diverging linewidth is due to the approximations necessary to arrive at our analytical results

(see above). This divergence is, in fact, already known to occur since the early work by Petermann,
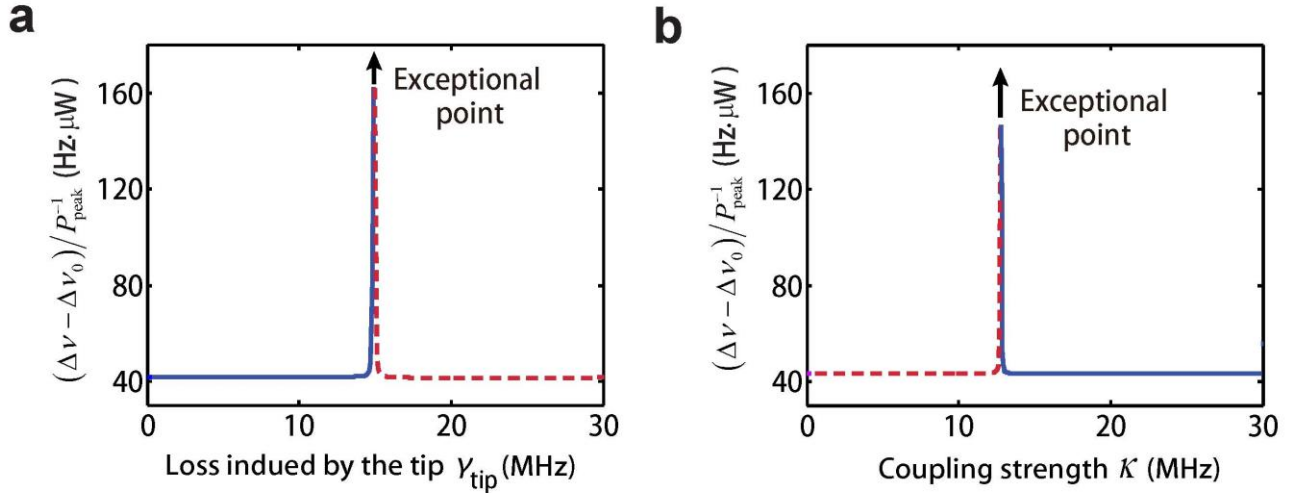
Figure S7. Normalized linewidth of the phonon laser $\left(\Delta v - \Delta v_0\right)/P_{\text{peak}}^{-1}$ **in the vicinity of the**

exceptional point. a, $\left(\Delta v - \Delta v_0\right)/P_{\text{peak}}^{-1}$ versus the tip-induced loss rate γ_{tip}. **b,** $\left(\Delta v - \Delta v_0\right)/P_{\text{peak}}^{-1}$ versus

the coupling strength κ. The normalized linewidth of the phonon laser is enhanced in the vicinity of the

exceptional point both in (a) and (b).

Siegmann etc. on the linewidth of the optical laser that shows the same divergence. We believe that the linewidth divergence at the EP can be tamed by a more rigorous theoretical approach along the lines of Ref. [S12] in which finite bounds on the enhancement in spontaneous emission at an EP have recently been presented. The challenge will be to merge this new approach with a linewidth calculation as presented above.

V.   NONDEGENERATE OPTICAL MODES

In this section, we want to briefly consider the case of non-degenerate (uncoupled) optical cavity resonance frequencies $\omega_1 \neq \omega_2$. Since the two optical modes a_1 and a_2 are coupled to each other, these two modes should be near-resonant. Thus, we can assume that $|\omega_1 - \omega_2| \ll \gamma, \kappa$. Additionally, in order to simplify our discussions, we only consider how this non-ideal case will affect our results in the vicinity of the exceptional point. Thus, we assume that $\beta, \tilde{\beta} \ll |\omega_1 - \omega_2|$. With the above two assumptions, Eqs. (S.4)-(S.6) can be reexpressed as

$$\begin{pmatrix} a_+ \\ a_- \end{pmatrix} = \mathcal{N}^{-1} \begin{pmatrix} \tau_+ & \tau_- \\ 1 & 1 \end{pmatrix}^{-1} \begin{pmatrix} a_1 \\ a_2 \end{pmatrix} = \mathcal{N}^{-1} \begin{pmatrix} \mu & -\lambda \\ -\mu & \lambda \end{pmatrix} \begin{pmatrix} a_1 \\ a_2 \end{pmatrix} \tag{S.90}$$

with complex eigenfrequencies

$$\omega_\pm \approx \omega_p - \omega_0 \pm \sqrt{\gamma |\Delta_-|} - i\chi, \tag{S.91}$$

where $\chi = (\gamma_1 + \gamma_2)/2$, $\gamma = (\gamma_2 - \gamma_1)/2$, $\omega_0 = (\omega_1 + \omega_2)/2$, $\Delta_- = (\omega_2 - \omega_1)/2$, and

$$\tau_\pm \approx \frac{\Delta_- + i\gamma}{\kappa} \pm \frac{\sqrt{\gamma |\Delta_-|}}{\kappa}(1+i) \approx \frac{i\gamma}{\kappa},$$

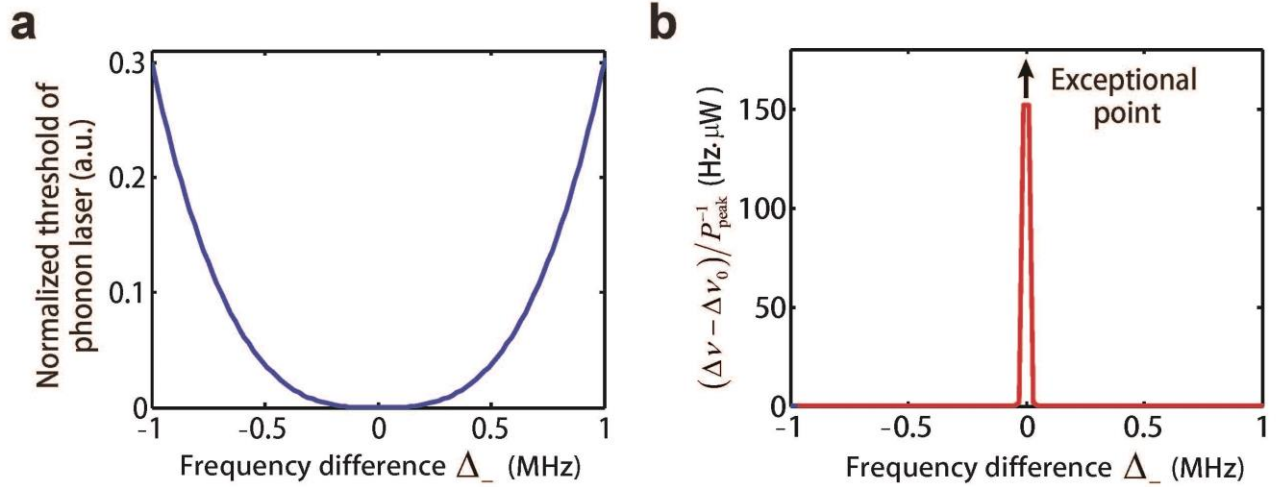$$\mu \approx \frac{(1-i)}{4} \sqrt{\frac{\gamma}{|\Delta_-|}},$$

$$\lambda \approx \frac{(1+i)}{4}\sqrt{\frac{\gamma}{|\Delta_-|}},$$

$$\mathcal{N} \approx \frac{1}{2}\sqrt{\frac{\gamma}{|\Delta_-|}}, \tag{S.92}$$

With similar discussions as those in Sec. III and Sec. IV, the threshold and linewidth of the phonon laser can be expressed as

$$P_{\text{threshold}} \approx \frac{16\hbar\Gamma_m \left(\gamma|\Delta_-|\right)^{3/2}\chi\left[\chi^2+\left(\Omega_m/2\right)^2\right]\omega_0}{\kappa^3 g_{om}^2 \Omega_m}. \tag{S.93}$$

$$\Delta\nu \approx \Delta\nu_0 + \frac{\Gamma_m}{2n_{b,ss}}\left\{\frac{g_{om}^2\kappa^4\chi}{16\gamma^2\Delta_-^2\left[\chi^2+\left(\Omega_m/2-\beta\right)^2\right]\Gamma_m}+2n_{bT}+1\right\}. \tag{S.94}$$

Figure S8. Threshold $P_{\text{threshold}}$ **and normalized linewidth of the phonon laser** $\left(\Delta\nu-\Delta\nu_0\right)/P_{\text{peak}}^{-1}$ **of the phonon laser versus the frequency difference** $\Delta_- =\left(\omega_2-\omega_1\right)/2$. **a,** Normalized threshold of the phonon laser versus Δ_-. **b,** $\left(\Delta\nu-\Delta\nu_0\right)/P_{\text{peak}}^{-1}$ versus Δ_-. The linewidth of the phonon laser decreases very fast in the vicinity of the resonant point $\Delta_- =0$.

Employing the system parameters $\Omega_m = 17.38$ MHz, $g_{om} = 1.5$ kHz, $\Gamma_m = 40$ kHz, $\gamma_1 = 3.16$ MHz,

$\gamma_2 = 13.56$ MHz, $\kappa = 12.63$ MHz, $\gamma_{tip} = 14.85$ MHz, we plot the curves of the phonon laser threshold and

the normalized linewidth of the phonon laser $\left(\Delta\nu - \Delta\nu_0\right)\big/P_{peak}^{-1}$ versus the frequency difference Δ_- in Fig.

S8. It is shown in Fig. S8b that the linewidth of the phonon laser decreases very fast in the vicinity of the

resonant point $\Delta_- = 0$.

VI.   LINEWIDTH BROADENING OF THE OPTICAL MODES NEAR THE EP

In order to obtain a physical understanding of the mechanism behind the linewidth broadening of the

phonon laser, we now take a closer look at the behavior of the optical modes in the vicinity of the EP.

Previous work has already demonstrated that the linewidth of an optical laser can be significantly

enhanced when the eigenmodes of the system are non-orthogonal [S13], [S14]. In our system, the lasing

mode is the mechanical mode while the optical modes are not lasing. As shown below, however, the non-

orthogonality of the optical modes in the vicinity of the EP still leads to an enhancement of the effective

optical noise strength.

Following a very simple approach, the two coupled optical modes present in our setup can be modeled by

a system of beamsplitters [S15], see schematic in Fig. S9a. In this picture the coupling strength between

the two optical modes a_1 and a_2 is determined by the reflection and transmission coefficients r and t.

Additionally, each of the two optical modes is coupled to a corresponding loss mode (c and d) via

beamsplitters with reflection and transmission coefficients r_i and t_i. All reflection and transmission

coefficients satisfy the relation $|r_i|^2 + |t_i|^2 = 1$. One roundtrip in this cavity is then described by the following four-mode unitary scattering matrix,

$$M = \begin{pmatrix} t\,t_1 & r\,t_1 & r_1 & 0 \\ -r\,t_2 & t\,t_2 & 0 & r_2 \\ -t\,r_1 & -r\,r_1 & t_1 & 0 \\ r\,r_2 & -t\,r_2 & 0 & t_2 \end{pmatrix}. \tag{S.95}$$

Since we are only interested in the optical modes a_1 and a_2, we reduce our considerations to the truncated scattering matrix for modes a_1 and a_2,

$$m = \begin{pmatrix} t\,t_1 & r\,t_1 \\ -r\,t_2 & t\,t_2 \end{pmatrix}, \tag{S.96}$$

which is sub-unitary and has non-orthogonal eigenvectors in general. With the help of Eq. (S.96), the input/output relations for the cavity roundtrip can be formulated as follows,

$$a_{1,\text{out}} = t\,t_1\,a_{1,\,\text{in}} + r\,t_1\,a_{2,\text{in}} + r_1\,a_{1,s}, \tag{S.97}$$

$$a_{2,\text{out}} = t\,t_2\,a_{2,\,\text{in}} - r\,t_2\,a_{1,\text{in}} + r_2\,a_{2,s}, \tag{S.98}$$

where the spontaneous emission noise contributions $a_{1,s}$ and $a_{2,s}$ are introduced to preserve unitarity. Under the simplifying assumption that a_2 is recoupled onto itself (i.e., $a_{2,\text{out}} = a_{2,\text{in}}$) it is straightforward to calculate the factor by which the noise acting on a_1 is enhanced as compared to the noise present in Eq. (S.97) alone (see Ref. [S15] for further details). This excess noise factor is the well-known Petermann factor given here by the following expression

$$K_1 = 1 + \frac{r^2 t_1^2 r_2^2}{r_1^2 \left(1 - t\,t_2\right)^2}. \tag{S.99}$$

Analogously, one can derive the noise enhancement factor for a_2, which is found to be

$$K_2 = 1 + \frac{r^2 r_1^2 t_2^2}{r_2^2 \left(1 - t\, t_1\right)^2}. \tag{S.100}$$

By applying the above formalism to our case, which is described by Eqs. (S.1) and (S.2) with $g_{om} = 0$ and

$\Delta \triangleq \omega_p - \omega_0$, we find

$$K_1 = 1 + \frac{\kappa^2 \gamma_2}{\gamma_1 \left(\Delta^2 + \gamma_2^2\right)}, \tag{S.101}$$

$$K_2 = 1 + \frac{\kappa^2 \gamma_1}{\gamma_2 \left(\Delta^2 + \gamma_1^2\right)}. \tag{S.102}$$

Fig. S9b shows the effective optical noise enhancement factor for our system parameters, where one can

observe a clear maximum of the curve at the EP, where the eigenmodes of the system are identical. Our

calculations thus reveal very clearly that the optical modes continuously increase their noise (i.e. their

linewidth) when approaching the EP (without a divergence occurring right at the EP). Since, in turn, the

mechanical mode in our phonon laser is driven by these noisy optical supermodes, this increase of the

optical noise power is then transferred to the mechanical mode through the optomechanical interaction

mechanism. As a result, also the mechanical (phonon) mode features a linewidth broadening when

approaching the EP.
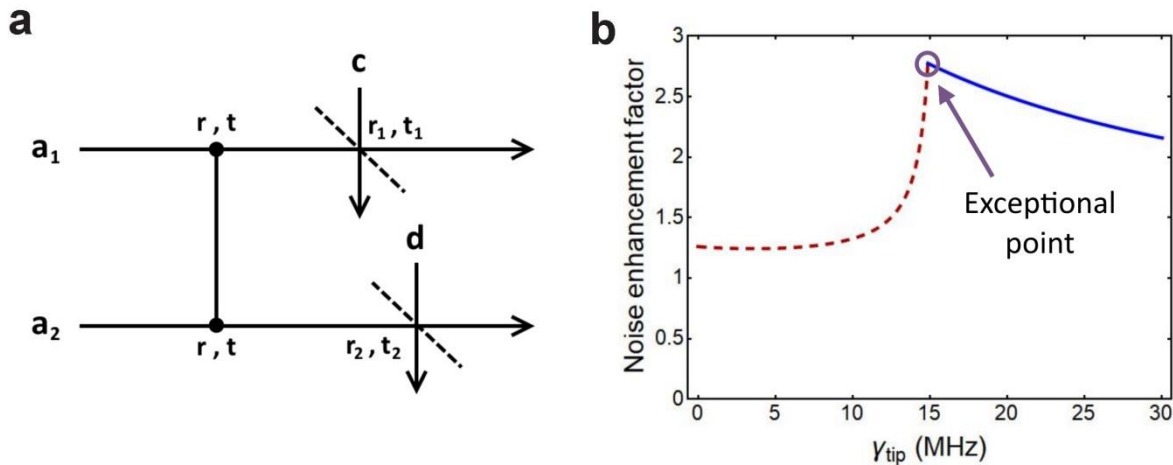
Figure S9. Simplified model for the linewidth broadening due to the non-orthogonality of the optical modes. a, The two optical modes a_1 and a_2 are coupled to two loss modes c and d via mirrors with reflection coefficients r_1 and r_2, and transmission coefficients t_1 and t_2, respectively. Furthermore, we assume a perfect coupling without coupling losses between a_1 and a_2, which is characterized by the reflection and transmission coefficients r and t. **b,** Optical noise enhancement as a function of the additional loss γ_{tip}. The effective optical noise strength features a clear maximum at the EP.

References:

[S1]   Grudinin, I. S., Lee, H., Painter, O. & Vahala, K. J. Phonon laser action in a tunable two-level system. *Phys. Rev. Lett.* **104**, 083901 (2010).

[S2]   Wang, H., Wang, Z. X., Zhang, J., Ozdemir, S. K., Yang, L. & Liu, Y. X. Phonon amplification in two coupled cavities containing one mechanical resonator. *Phys. Rev. A* **90**, 053814 (2014).

[S3]   Mahboob, I., Nishiguchi, K., Fujiwara, A. & Yamaguchi, H. Phonon lasing in an electromechanical resonator. *Phys. Rev. Lett.* **110**, 127202 (2013).

[S4]   Jing, H., Ozdemir, S. K., Lü, X.-Y., Zhang, J., Yang, L. & Nori, F. PT-symmetric phonon laser. *Phys. Rev. Lett.* **113**, 053604 (2014).

[S5]   Jing, H., Ozdemir, S. K., Geng, Z., Zhang, J., Lü, X.-Y., Peng, B., Yang, L. & Nori, F. Optomechanically-induced transparency in parity-time-symmetric microresonators. *Sci. Rep.* **5**, 9663 (2015).

[S6]   Schonleber, D. W., Eisfeld, A. & El-Ganainy, R. Optomechanical interactions in non-Hermitian photonic molecules. *New J. Phys.* **18**, 045014 (2016).

[S7]   Walls, D. F. & Milburn, G. J. *Quantum Optics* (Springer, Berlin, 1994).

[S8]   Bergli, J., Galperin, Y. M. & Altshuler, B. L. Decoherence in qubits due to low-frequency noise. *New J. Phys.* **11**, 025002 (2009)

[S9]   van Exter, M. P., Kuppens, S.J.M. & Woerdman J. P. Theory for the linewidth of a bad-cavity laser. *Phys. Rev. A* **51**, 809-816 (1995).

[S10] Haken, H. Light: Laser Light Dynamics (North-Holland, Amsterdam, 1985), vol. 2.

[S11] Scully, M. & Zubairy, M. Quantum Optics (Cambridge University Press, Cambridge, 1997).

[S12] A. Pick, B. Zhen, O. D. Miller, C. W. Hsu, F. Hernandez, A. W. Rodriguez, M. Soljacic, S. G. Johnson, General theory of spontaneous emission near exceptional points. *Opt. Exp.* **25**, 12325-12348 (2017).

[S13] K. Petermann. Calculated spontaneous emission factor for double-heterostructure injection lasers with gain-induced waveguiding. *IEEE J. Quantum Electron.* **15**, 566 (1979).

[S14] A. E. Siegman. Excess spontaneous emission in non-Hermitian optical systems. *Phys. Rev. A* **39**, 1253 (1989).

[S15] Ph. Grangier and J.-Ph. Poizat. A simple quantum picture for the Petermann excess noise factor. *Eur. Phys. J. D* **1**, 97–104 (1998).